Oxygen interaction at Ag(511): from chemisorption to the initial stages of oxide formation

2008 J. Phys.: Condens. Matter 20 224006

(http://iopscience.iop.org/0953-8984/20/22/224006)

J. Phys.: Condens. Matter **20** (2008) 224006 (9pp) doi:10.1088/0953-8984/20/22/224006

Oxygen interaction at Ag(511): from chemisorption to the initial stages of oxide formation

L Savio[1,2,5], **C Giallombardo**[1,2], **L Vattuone**[1,2], **A Kokalj**[3] **and M Rocca**[1,4]

[1] Dipartimento di Fisica, Università di Genova, Via Dodecaneso 33, 16146 Genova, Italy
[2] CNISM, Unità di Genova, Via Dodecaneso 33, 16146 Genova, Italy
[3] Jožef Stefan Institute, Jamova 39, Ljubljana, Slovenia
[4] IMEM/CNR, Via Dodecaneso 33, 16146 Genova, Italy

E-mail: savio@fisica.unige.it

Received 8 November 2007
Published 13 May 2008
Online at stacks.iop.org/JPhysCM/20/224006

Abstract
We report here on a combined experimental and computational investigation of oxygen interaction with Ag(511), a vicinal surface of Ag(100) characterized by a high density of close-packed steps. The different adsorbed species, either molecular or dissociated, and their reactivity towards CO are characterized by vibrational and photoemission spectroscopy, while the possible adsorption sites are determined by density functional theory calculations. The initial phases of Ag_2O nucleation are also observed; the role of step geometry in the oxide formation process is discussed in comparison with previous results for Ag(210).

(Some figures in this article are in colour only in the electronic version)

1. Introduction

Oxygen interaction with Ag surfaces has been investigated thoroughly in the past, searching for the oxygen moiety active in the ethylene epoxidation reaction. Such a process is catalysed by Ag powders with a unique selectivity with respect to the alternative channel of total combustion [1] and occurs routinely in industrial conditions. In spite of this, it could never be reproduced under controlled UHV conditions, so that the elementary steps of the reaction are still unclear and the active oxygen species has escaped identification so far. In this frame the role of defects for the O_2/Ag interaction is particularly intriguing since the system is known to be structure sensitive [2, 3] and since we have recently demonstrated that the O_2 adsorption and dissociation barriers are heavily reduced for Ag(410) and Ag(210) [4, 5]. Moreover, on the latter surface, O-induced relaxation leads to subsurface migration of O atoms [5–7]. Ag(410) and Ag(210), consist, respectively, of 3 and 1 atom row wide (100) nanoterraces alternated with (110)-like monatomic step rises and show therefore an open step profile with 25% and 50% of under-coordinated sites. The choice of such geometry was guided by the suggestion, gained in previous O_2 adsorption experiments on flat and sputtered Ag(100), that kinks are indeed the active sites for O_2 dissociation [8]. Moreover, Ag(410) is well known to be the stable, faceted phase of Ag(100) upon massive O_2 exposure [9].

The initial oxidation of noble and transition metal surfaces has been the subject of extensive theoretical [10–12] and experimental [13, 14] research over the last years. Such interest is motivated both by the seeking of a fundamental understanding of the crossover between surface chemisorption and oxide formation and by the relevance of oxide surfaces for a wide set of applications, ranging e.g. from catalysis [15, 16] to fabrication of nanoparticles with special non-linear optical properties [17]. In spite of the many efforts, however, the phenomenon is not yet completely understood. E.g., the structure of O/Ag(111) has been recently revised [18, 19], suggesting that it consists in a chemisorbed phase rather than in a surface oxide layer, as previously proposed [20].

Recent experimental and theoretical works [10, 21, 22] pointed out the existence of a critical coverage for the transition from chemisorbed on-surface phases to the growth of oxidic films. Carlisle *et al* [21] proposed that the transition is

[5] Author to whom any correspondence should be addressed.

determined by the steep decrease of the heat of adsorption with increasing surface coverage. Such reduction is due to the repulsive lateral interactions between adsorbates, which makes oxide formation energetically more favoured than adsorption of extra oxygen atoms at surface sites. Indeed, it was demonstrated [10] that the energy gain due to oxide formation counterbalances the energetic costs of lattice deformation required for O incorporation in subsurface sites.

Ag oxides exist in two different stoichiometries, Ag_2O (cubic) and AgO (monoclinic), characterized by vibrations at 525 cm^{-1} (66 meV) and 410–450 cm^{-1} (51–56 meV), respectively [11, 23, 24]. O atoms occupy the tetrahedral interstitials in Ag_2O and an off-centre position of the octahedral sites in AgO. No signatures of oxide formation were ever reported for ultra-high vacuum experiments upon oxygen exposure on perfect low Miller index Ag faces [25–27][6] and on Ag(410) [4], while a loss at 53–56 meV was detected upon oxygen exposure on Ag(210) [5–7, 28]. Such vibration corresponds to the in-phase displacement of O atoms at the step and in the octahedral interstitial underneath it against the Ag lattice (i.e. to a Fuchs–Kliever-like motion in oxides) and thus indicates an easy access of O atoms into the subsurface region. Subsurface site occupation occurs already at a crystal temperature $T = 110$ K and is stable up to just below room temperature (RT) [5, 28]. Since the phenomenon does not occur for Ag(410), both the presence of the steps and the relaxation allowed by the very limited (100) terrace width prove to be essential. More recently, high resolution x-ray photoemission spectroscopy (XPS) experiments [28] allowed us to distinguish the super- and subsurface oxygen moieties on Ag(210) from the point of view of their binding energy, E_B, which is 527.7 eV and 529.6 eV, respectively. The former value is close to the one reported for Ag(110) and Ag(111) [29, 2], and for Ag(100) above room temperature [25]. The latter is intermediate between bulk silver oxide ($E_B(Ag_2O) = 528.9$ eV [30, 31]) and subsurface oxygen ($E_B(O_{sub}) = 531$ eV [25, 32, 33]) and is similar to that reported for other Ag surfaces [34, 35] following O_2 exposures at higher pressure.

Here we report on a complete high resolution electron energy loss spectroscopy (HREELS), x-ray photoemission spectroscopy (XPS) and density functional theory (DFT) investigation of the O_2 interaction with Ag(511). At variance with the previously investigated (n10) surfaces, Ag(511) is characterized by a 33% density of close-packed steps, and a different behaviour towards O_2 dissociation is thus expected. Indeed we observe low temperature dissociation also on this surface, probably induced by secondary defects at the intrinsic steps, and a variety of adsorption sites which are populated depending on experimental conditions and identified by DFT. More interestingly, we find that the close-packed geometry also induces oxygen accumulation in subsurface sites and that the initial nucleation of a surface oxide phase shows the vibrational signature of Ag_2O. The role of step geometry in the oxide formation process is then discussed in comparison with the previous results for O/Ag(210).

[6] The paper reports on a complete HREELS and DFT investigation of the vibrational modes of O/Ag(100). We observed a tiny loss at 67 meV, tentatively assigned to the parallel vibration of O predicted at 59 meV. In view of the present results the assignment should be revised and the loss attributed to oxide nucleation at defects. Close-packed steps are indeed expected to be the most common defect at Ag(100).

2. Experimental and computational methods

Experiments were performed in ultra-high vacuum (UHV), at a base pressure better than 3×10^{-10} mbar. The apparatus is equipped with a quadrupole mass spectrometer for gas analysis, a low energy electron diffractometer (LEED), an ion gun for *in situ* cleaning of the sample, a commercial HREELS (Specs) and a hemispherical analyser for x-ray photoemission spectroscopy (Omicron). O_2 and CO are dosed by backfilling the chamber.

HREEL spectra are recorded in-specular, at an incidence angle $\theta_i = 54°$ or 62° from the surface normal and with a primary electron energy $E_e = 2.0$ eV. The typical resolution is between 3.5 and 6.0 meV, depending on surface conditions. XPS spectra are acquired using a conventional Mg Kα x-ray source ($h\nu = 1253.6$ eV) and collecting the photoemitted electrons at an emission angle of 72°. The binding energy of the XPS peaks, E_B, is calibrated by fixing the $Ag3d_{5/2}$ line to 368.25 eV, in accord with the value reported in the literature [36].

The O coverage, Θ, is estimated from the XPS intensity upon calibration of the O 1s signal on the (3×1)O–Ag(110) added row reconstruction and after correcting for the different surface density of Ag(511) with respect to Ag(110) (1.13×10^{15} atoms cm^{-2} and 0.85×10^{15} atoms cm^{-2}, respectively). The relative error on the estimated intensity/coverage is between 5% and 20%, depending on the quality of the original spectra. The relative sensitivity to O and C is assumed to be ~2.4 from the ratio of the photoemission cross sections [37].

The Ag(511) sample is a disc of 10 mm diameter. It is cleaned by sputtering with Ne ions followed by annealing to a crystal temperature $T = 740$ K until no traces of contaminants appear in the HREEL spectra and a good surface order is detected by LEED inspection. In these conditions XPS shows a residual peak around $E_B = 284$ eV. It must correspond to some contamination by C atoms in a subsurface location (estimated in ~0.07 ML distributed over several Ag layers) since the binding energy is suitable for isolated C and the intensity cannot be removed either by prolonged sputtering or by O_2 treatment at high T. The surface geometry is schematically reported in figure 1: it consists of 3 atom row wide (100) nanoterraces alternated with (111)-like monatomic steps running in the $\langle 0\bar{1}1 \rangle$ direction. Therefore, intrinsic steps show a close-packed configuration and are expected to be poorly reactive.

DFT calculations are performed using the PBE energy functional [38]. We have used the pseudopotential method with ultra-soft pseudopotentials [39] and plane-wave basis set up to a kinetic-energy cut-off of 27 Ryd (216 Ryd for the charge-density cut-off). Brillouin zone (BZ) integrations have been performed with the special-point Gaussian smearing technique using a smearing parameter of 0.03 Ryd. Calculations have been done with the PWscf code contained in the Quantum ESPRESSO package [40], while molecular graphics were generated using the XCRYSDEN program [41]. The Ag(511)

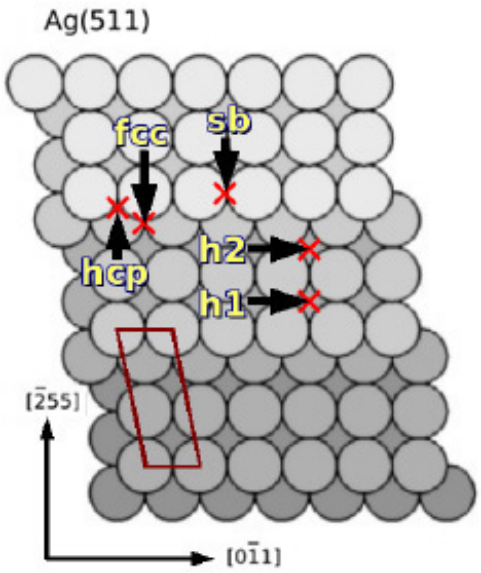

Figure 1. Structure of the Ag(511) surface. The primitive unit cell and the crystallographic directions are indicated, too. Ag(511) is formed by 2 atomic row wide (100) terraces separated by monatomic (111)-like steps, so that 33% of atoms are under-coordinated. Surface sites considered in this work are marked by crosses.

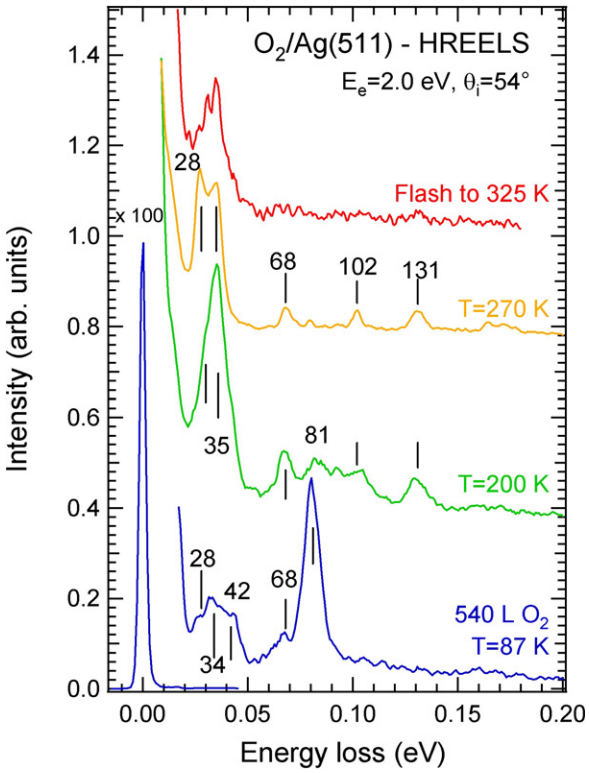

Figure 2. Sequence of HREEL spectra recorded after dosing 540 L of O_2 on Ag(511) at $T = 87$ K and after subsequent annealing to 200, 270 and 325 K. The surface was re-cooled to 87 K to record the spectra.

surface was modelled with slabs consisting of 14 (511) layers separated by a vacuum layer of about 15 Å thickness with the bottom three layers fixed (the remaining degrees of freedom

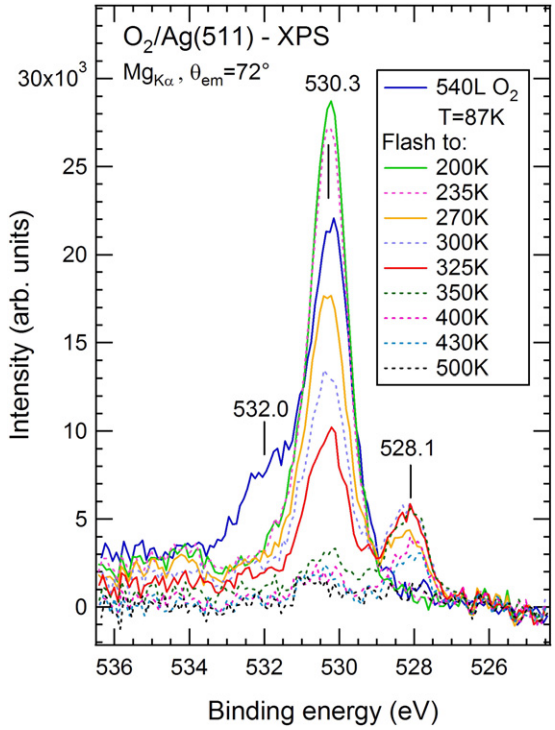

Figure 3. Sequence of XPS spectra recorded after preparing the O-layer as in figure 2. Continuous lines correspond to the same annealing temperatures as the HREELS experiment, dotted ones to intermediate temperatures.

were optimized). Adsorption has been modelled by (2 × 1) surface super-cells using a (5 × 4 × 1) uniformly shifted k-mesh for the BZ integration.

3. Results

Typical HREELS and XPS experiments in which 540 L of O_2 are dosed on Ag(511) at $T = 87$ K and the crystal is then annealed to different T are reported in figures 2 and 3, respectively. The vibrational loss at 81 meV is due to the intermolecular stretch of O_2 admolecules in the peroxide state [42], while the peaks at 28–42 meV are characteristic of oxygen adatoms [8]. Partial dissociation occurs therefore already at temperatures at which only molecular chemisorption takes place on Ag(100) and Ag(110). This outcome is similar to the case of O_2/Ag(410) and indicates that little or non-activated dissociative adsorption channels also open up at close-packed steps. The efficiency of this process is however reduced with respect to Ag(n10) surfaces, as witnessed by the low initial sticking probability, S_0, measured for O_2/Ag(511): at 110 K and with a supersonic O_2 molecular beam of translational energy 0.97 eV impinging at normal incidence, $S_0 = 0.34$ and it drops extremely rapidly to 0.08 [43]. For comparison, in similar conditions $S_0 = 0.60$ for Ag(100) and Ag(410) and $S_0 = 0.45$ for Ag(210) with no rapid drop with coverage. Low T dissociation on Ag(511) is therefore likely to occur at secondary defects, presumably kinks at steps showing an open geometry. Going back to the HREEL spectrum, we note that the inelastic intensity at 68 meV is

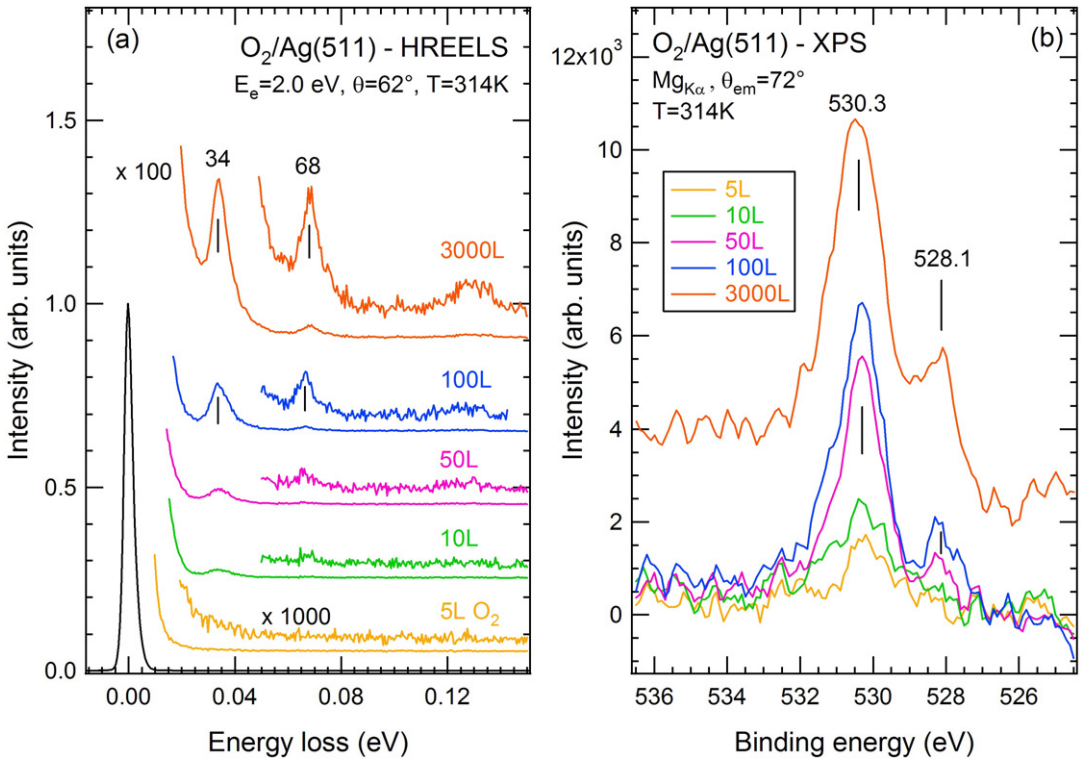

Figure 4. Oxygen uptake at $T = 314$ K monitored by HREELS (a) and XPS (b).

particularly intriguing since it is suitable for subsurface oxygen and in particular for Ag_2O formation. The corresponding XPS spectrum exhibits a main O 1s peak at $E_B = 530.3$ eV (O530) and a shoulder around $E_B = 532$ eV. The former intensity arises from the unresolved contributions of all molecular and atomic species. O_2 was indeed reported at 529.7 eV both for Ag(100) [44] and for Ag(110) [29], while covalent O was reported at $E_B = 530.3$ eV for Ag(100) [25]. The high energy feature, on the contrary, is due most probably to a small water contamination [45], since it disappears in the temperature range typical of OH formation and a small OH stretch is visible at 445 meV in the HREEL spectra (not shown).

Flashing the crystal to 200 K, most of the O_2 desorbs and/or dissociates, as witnessed by the strong reduction of the 81 meV peak and by the growth of the intensity at 35 meV in the HREEL spectrum. The 42 meV (if still present) and the 28 meV vibrations are now hidden in the major peak. The 68 meV feature is more intense and well defined, while a new structure appears at 131 meV. It has already been reported for Ag(100) and ascribed to an electronic transition in oxide clusters [46]. The additional small peak at 102 meV indicates little carbonate formation, also confirmed by XPS inspection of the C 1s region [29]. The XPS intensity at 530.3 eV increases, indicating that some subsurface O segregation must take place as in the case of O/Ag(210) [28]; this point will be discussed in more detail in the following.

After further heating to 270 K the HREEL spectrum is characterized by the growth of the 28 meV loss while the 35, 68 and 131 meV peaks decrease in intensity; annealing to 325 K causes the disappearance of the last two features and a strong reduction of the low frequency ones. The corresponding XPS spectra show the formation of a new moiety with $E_B = 528.1$ eV (O528), which initially is not associated with a reduction of the 530.3 eV intensity. O530 is totally depleted at 350 K while the O528 species is populated up to 430 K. Finally, we note that the O528 intensity anticorrelates with that of the 68 meV vibration.

Figure 4 reports the HREELS (panel (a)) and XPS (panel (b)) spectra recorded during O_2 uptake experiments performed at 314 K. Only dissociative adsorption takes place at this T, as witnessed by the absence of any energy loss around 80 meV. The first traces of O adsorption are detected after an exposure $\chi = 5$ L by XPS (peak at 530.4 eV) and after $\chi = 10$ L by HREELS (peak at 34 meV). After 50 L of O_2, both the 68 meV loss and the photoemission signal at 528.1 eV are evident; further dosing causes the energy losses at 34 and 68 meV to grow in intensity, maintaining their frequency unchanged. The O530 and O528 features also increase, although with very different rates: the high energy peak grows more rapidly in the initial stages of the exposure, while the low energy one shows a much slower and more linear increment. The oxygen coverage, as evaluated from the analysis of the XPS intensities, is reported in figure 5. Diamonds and squares represent the partial coverages of O530 and O528 versus χ; the red circles are the sums of the two contributions and represent therefore the total coverage (O_{tot}). The arrows indicate the coverage values after dosing 3000 L of O_2. We underline that carbonate formation, which contributes to the 530.3 eV intensity, is negligible at $T = 314$ K. Initially, almost only O530 forms. The Θ/χ ratio allows us to evaluate the average adsorption probability, S, after a fixed exposure. We find $S \sim 0.015$ after 5 L, which is the best available approximation for the

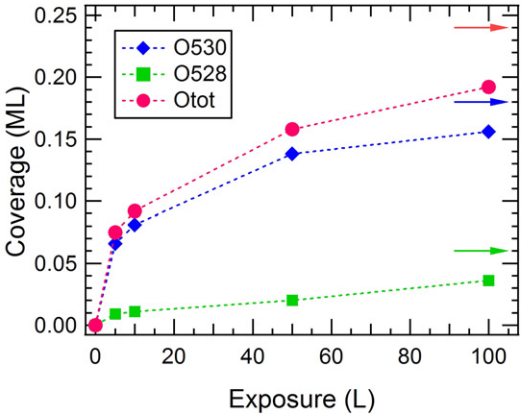

Figure 5. Coverage versus exposure curves for the O530 and the O528 XPS intensities and for their sum (O_{tot}). The arrows indicate the coverage achieved for $\chi = 3000$ L.

initial sticking coefficient, and $S \sim 2 \times 10^{-3}$ and 8×10^{-5} for $\chi = 100$ L and 3000 L, respectively. Such low values are coherent with the reduced reactivity of Ag(511) with respect to stepped surfaces with open step geometry.

Finally, we probed the reactivity of the different O species towards CO oxidation. An O layer is produced by dosing 100 L of O_2 on Ag(511) at 314 K and is exposed to 50 L of CO at the same T (see figure 6). Such treatment causes no apparent changes in the HREEL spectrum (panel (a)), except for a slight increase of the 34 meV loss intensity. On the contrary, the same experiment monitored by XPS shows a strong reduction of the O528 peak after only 1 L of CO. No CO_3 formation is detected after such a short dose within our experimental sensitivity. Analogous results are obtained if the CO dose is performed with the sample cooled at 110 K. Such behaviour clearly indicates that O530 is completely inert towards CO oxidation while the low E_B moiety is highly reactive. Since at least one adatom species contributes to the intensity of the O530 peak, the observed behaviour gives evidence that not all adatoms react with CO, in contrast to the case of O/Ag(210) [47]. We also mention that CO_3 shows vibrational modes around 38 meV on Ag(210) [47]; some CO_3 formation and similar vibrational frequencies could justify the small increase of the 34 meV loss intensity observed by HREELS. On the other hand, the O–Ag vibration of the reactive oxygen species is either not detected by HREELS or it superimposes with those of the O530 and/or carbonate species, so that its removal upon CO oxidation is hidden.

For a correct identification of the adsorption sites populated on Ag(511) we performed DFT calculations on the O/Ag(511) system. Moreover, in order to understand the role of steps in the nucleation of oxide phases, we compared these results with those available for O/Ag(210). Five different on-surface sites, defined in figure 1, have been investigated. Three of them are at the step: fcc, hcp, and the bridge (sb) directly on the step edge. The other two are fourfold hollow sites, marked as h1 (closest to the upper step edge) and h2 (closest to the bottom of the step), respectively. The corresponding average chemisorption energy per oxygen atom was calculated as

$$\langle E_{\mathrm{chem}} \rangle = [E_{\mathrm{O/surf}} - E_{\mathrm{surf}} - (N_{\mathrm{O}}/2)E_{\mathrm{O2}}]/N_{\mathrm{O}} \qquad (1)$$

where $E_{\mathrm{O/surf}}$, E_{surf}, and E_{O2} are the total energies of the oxygen/surface, surface, and oxygen molecule, respectively,

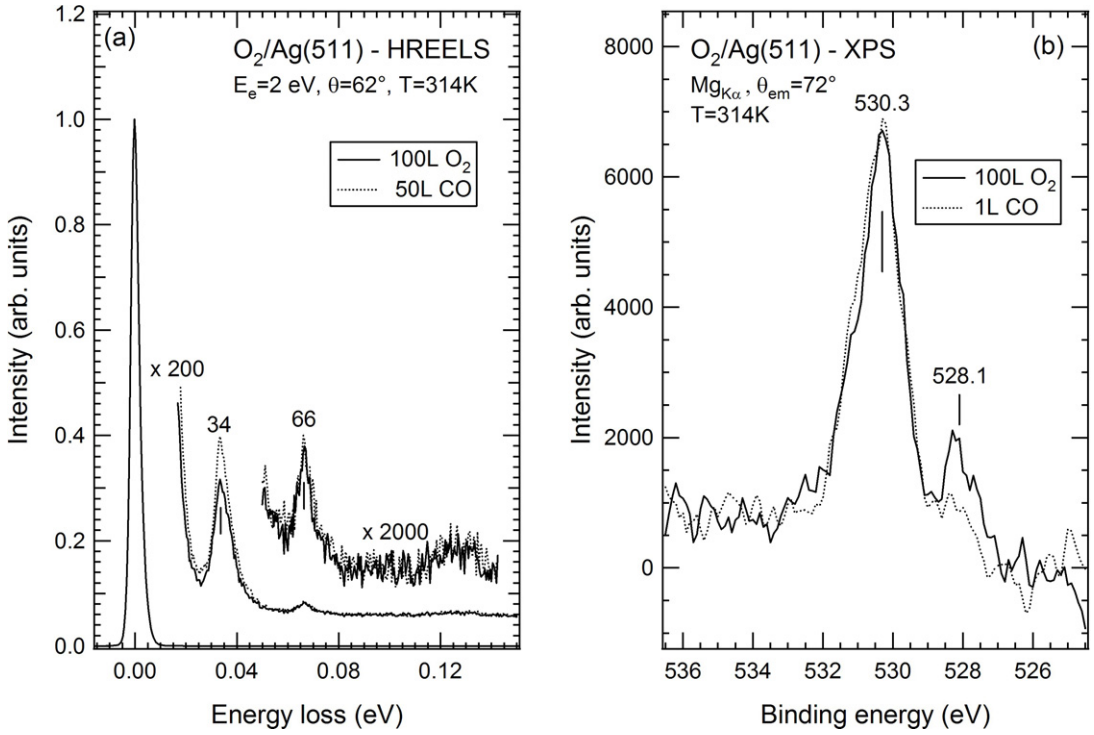

Figure 6. HREELS (a) and XPS (b) spectra recorded before and after exposure of the same O layer to CO. While no significant changes appear in the vibrational spectrum after 50 L of CO, almost complete removal of the O528 species is observed by XPS after only 1 L of exposure.

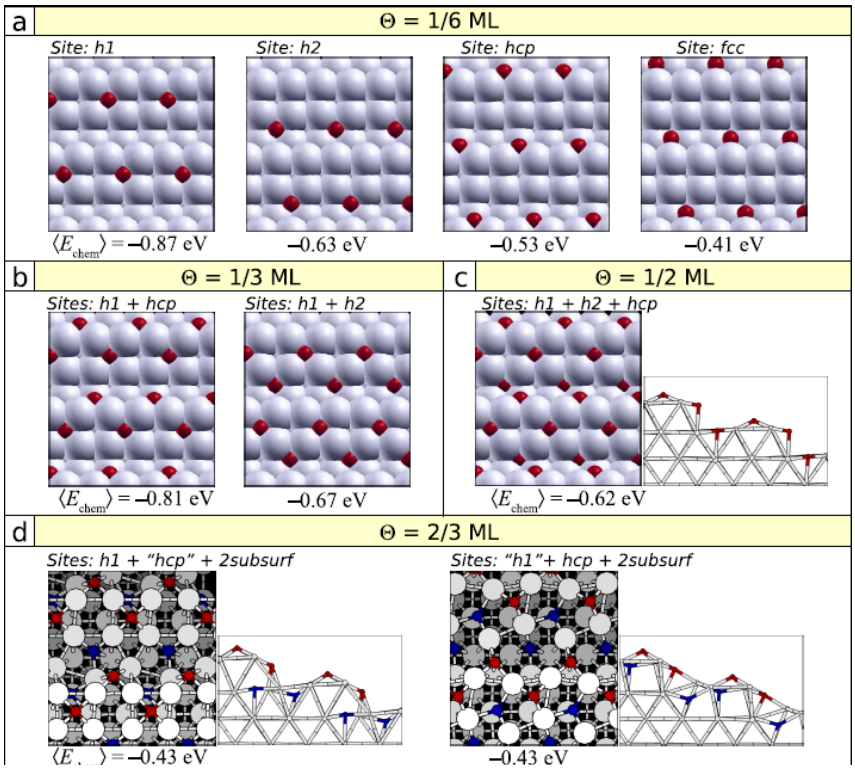

Figure 7. A subset of optimized O/Ag(511) structures (O atoms—small dark balls, Ag—big bright balls) and corresponding average chemisorption energies, $\langle E_{\rm chem}\rangle$, as a function of oxygen coverage, $1/6 < \Theta < 2/3$ ML: (a) top view of all identified stable O sites at low coverage, $\Theta = 1/6$ ML; (b) top view of two most stable structures at $\Theta = 1/3$ ML; (c) top and side view of the most stable structure at $1/2$ ML; (d) top and side view of two most stable, degenerate structures at $2/3$ ML. Note a significant deformation of the substrate lattice, which makes an assignment of sites difficult: the labels 'hcp' and 'h1' merely indicate the initial position of corresponding O atoms, whereas label *subsurf* indicates oxygen located into subsurface sites. (Online colour: on-surface oxygen is red; subsurface oxygen is blue.)

and $N_{\rm O}$ is the number of adsorbed oxygen atoms. We have considered about 30 different O/Ag(511) configurations in the coverage range between $1/6$ and $2/3$ ML. In figure 7 we show the optimized structures for some of them together with the corresponding $\langle E_{\rm chem}\rangle$. The suggested picture is that, at low O coverage ($\Theta = 1/6$ ML), the stability of sites follows the order h1 > h2 > hcp > fcc (see figure 7(a)), whereas sb is a saddle point connecting the h1 and hcp sites. At equilibrium, therefore, oxygen atoms first occupy the h1 sites. Note that, due to lateral electrostatic repulsion, oxygen atoms avoid occupying nearest-neighbour sites. This implies that after half of the h1 sites are occupied O atoms start to adsorb into other sites, in particular into hcp sites ($1/6$ ML $< \Theta \leqslant 1/3$ ML), forming zigzag chains across the step edge. Although the second most stable site at low coverage is h2, the zigzag chains are more stable than the combination of h1 + h2 sites (see figure 7(b)). The $\langle E_{\rm chem}\rangle$ of the zigzag chain (-0.81 eV) is more exothermic than the average of the two individual $\langle E_{\rm chem}\rangle$ at low coverage ($\frac{1}{2}(-0.87 - 0.63)$ eV $= -0.75$ eV). This is reminiscent of a very stable oxygen step edge decoration found on Ag(210) and Ag(410) [6, 48]. After half of h1 and hcp sites are occupied, O atoms start to adsorb into h2 sites ($1/3$ ML $< \Theta \leqslant 1/2$ ML). Figure 7(c) shows the most stable identified structure at $\Theta = 1/2$ ML. Only above this coverage, it is more convenient for additional oxygen atoms to migrate below the surface, where they end up in distorted four- and fivefold coordinated sites, some of which may resemble highly deformed tetrahedral and octahedral sites, respectively. The inclusion of oxygen below the surface induces a substantial deformation of the substrate lattice. In figure 7(d) we show the two most stable identified structures at $\Theta = 2/3$ ML, which are energetically degenerate. Among the considered structures at this coverage, we have also identified one with the O atoms located into less distorted octahedral sites, which is slightly less stable by 0.1 eV. This finding is at variance with the case of Ag(210) where the off-centre octahedral site is the most stable. On Ag(511) the nucleation of an Ag_2O-like surface phase—characterized by tetrahedral site occupation—is thus energetically slightly preferred with respect to the formation of an AgO-like one [49]. We notice that the $\Theta = 2/3$ ML configurations correspond to a higher (less exothermic) enthalpy, calculated as $\Delta H \approx N_{\rm o}\langle E_{\rm chem}\rangle$, than the $\Theta = 1/2$ ML one, which contains only supersurface O. According to our simulations, oxide may thus form only under non-equilibrium conditions and is not expected to survive annealing, in agreement with the poor thermal stability observed experimentally. Moreover, the configurations achieved experimentally at low T might not correspond to the equilibrium conditions computed by DFT, but rather to the occupation of metastable sites.

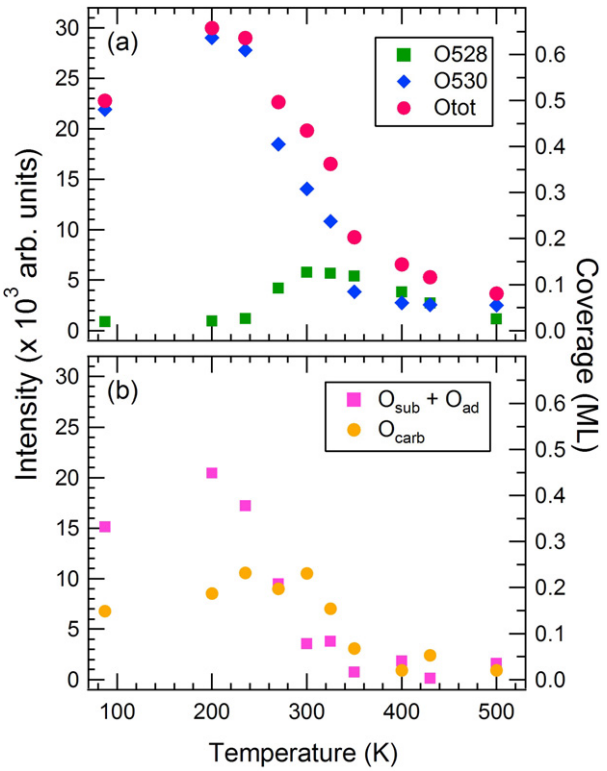

Figure 8. (a) Behaviour of the O530, O528 and O_{tot} intensity as a function of annealing temperature. (b) Contributions of the O_{carb} and of O atoms in super- and subsurface locations to the O530 peak. Segregation from the deep subsurface layers when annealing to 200 K is evident. The corresponding coverage, as estimated from the XPS intensity, is reported on the right axis (expressed in density of O atoms also for O_{carb}).

4. Discussion

Figure 8 reports a detailed analysis of the XPS intensities versus T as recorded in the experiment of figure 3[7]. As already remarked, the O530 intensity grows by ∼30% upon annealing the O layer to 200 K. Since no additional adsorption occurs from the gas phase, such behaviour is indicative of oxygen segregation from the deep subsurface layers, similarly to what is observed for O/Ag(210). O530 is stable up to ∼250 K and disappears completely at ∼350 K. The O528 species, in contrast, grows between 250 and 300 K and remains eventually stable up to 400 K.

During O_2 exposure some interaction of oxygen adatoms with the residual CO present in the UHV chamber causes CO_2 production. Adsorbed CO_2 is unstable but, at low T, its residence time is long enough to allow for some further oxidation into CO_3. Carbonate is therefore the main contaminant of the O/Ag layer [28]. These molecules are characterized by E_B(O 1s) = 530.3 eV and E_B(C 1s) = 287.7 eV [29] and their intensity adds therefore to the one of O530. However, once the O/C detection ratio is known [37] such contribution can be calculated from the corresponding C 1s signal through the formula $I(O_{CO3}) = I(287.7\ \text{eV}) \times 2.4 \times 3$, considering that in CO_3 there are three O atoms for each C atom. The contributions of oxygen atoms in super- and subsurface sites, I(O), results therefore from the difference $I(O) = I(530.3\ \text{eV}) - I(O_{CO3})$. Such analysis is reported in figure 8(b), in which the squares represent only the sum of oxygen atoms in super- and subsurface locations. Such a curve confirms that oxygen segregation occurs when annealing the layer to 200 K, while the oxygen signal decreases rapidly below RT. Carbonates (circles) are already present at 87 K; their coverage increases slightly during the first annealing and then remains stable up to 325 K. Such behaviour is coherent with that observed for O/Ag(210) [28]. Although in this case the interpretation of the data was simpler since super- and subsurface O had different binding energies, both results strongly indicate that interchange between the near- and the deep-subsurface region occurs. Since on Ag(511) no segregation is observed without O_2 exposure, subsurface oxygen is most probably stabilized by the presence of a critical supersurface oxygen coverage also on this crystal face. DFT supports this conclusion, suggesting that O_{sub} occupation is favoured above a critical coverage of 0.5 ML.

Although theoretical vibrational frequencies of the O/Ag(511) system and their consequent direct comparison with the experimental values are not available at the moment, the information derived from the calculations of the energetics of the system allows us to ascribe the HREELS and XPS peaks to the different adsorption sites. The assignment is summarized in table 1 and it is based on the following arguments.

(a) O dissociation at 87 K occurs at the step. The thus-generated adatoms must then sit close to it and have a covalent nature, since only O530 is detected by XPS. Annealing to 200 K causes complete dissociation and an increase of the 35 meV species, while the 42 meV peak disappears. On these bases we propose that the 34–36 meV frequency corresponds to O atoms at the h1 site, which is populated first according to DFT calculations. The 42 meV species, which is observed only at low T, must be related to adsorption at a metastable site, populated immediately after O_2 dissociation. Indeed, such intensity is depleted as soon as the adatoms have enough thermal energy to move to a more stable configuration.

(b) Some intensity at 28 meV is present already at low T. At 87 K a minor contribution to this loss might derive from the O_2/Ag mode of undissociated molecules, which is however expected to be small compared to the O–O

Table 1. Suggested correspondence among the observed vibrational frequencies and O 1s binding energies and the adsorption sites proposed by DFT.

Site	Vibrational frequency (meV)	E_B (eV)
h1	34–36	530.3
hcp	28	530.3
h2	34	528.1
Metastable	42	530.3

[7] A similar analysis performed on other XPS series, also in the absence of the initial small H_2O contamination, gives identical results, so figure 8 is representative of a general behaviour.

stretch. Since this vibration alone does not justify the whole intensity at 28 meV, a further, covalent atomic oxygen moiety must form already at 87 K. The 28 meV peak population is reinforced upon annealing to 200 K and even more upon reaching 270 K. We propose that it corresponds to O adatoms at hpc sites, which are populated immediately after the h1 ones.

(c) Above 235 K, O528 appears in XPS spectra, indicating the formation of a new atomic oxygen species. The assignment of this moiety is more complicated since it appears only close to RT and its intensity anticorrelates with that of the 68 meV peak in the HREEL spectra. We propose therefore that this oxygen, more oxidic in nature, forms from the dissolution of the surface oxide phase and sits in the h2 sites, i.e. at the height of the terrace plane and therefore close to the tetrahedral interstitials, which would be occupied in an Ag_2O-like configuration. The supersurface nature of the 528.1 eV species is witnessed by its high reactivity towards CO.[8] The corresponding vibrational frequency is around 35 meV in view of the fourfold symmetry of the adsorption site and of the absence of evident changes in the HREEL spectra upon CO oxidation. Oxygen at h1 and h2 sites shows similar coordination so that very close vibrational frequencies are expected; we suggest that the covalent or oxidic nature may be related to the presence of O in subsurface sites.

(d) The thermal behaviour of the Ag_2O vibration at 68 meV indicates that the oxide contributes to the O530 signal. In contrast to the case of O/Ag(210), however, such a contribution could not be resolved due to the presence of adatoms having a very close binding energy.

The critical coverage for subsurface site occupation on Ag(511) predicted by DFT is close to 0.5 ML, thus in good agreement with the one estimated from XPS experiments (see figure 8) and similar to the one predicted for O/Ag(210) [7]. Noteworthily, there are differences concerning the most stable subsurface site between the two surfaces: for Ag(210) the octahedral site is ≈0.2 eV more stable than the distorted tetrahedral site, whereas on Ag(511) we identify several structures of similar stability with the oxygen atoms located in distorted four- and fivefold coordinated subsurface sites, some of which resemble highly distorted tetrahedral and octahedral sites. Other structures involving O in less distorted octahedral sites are less stable by ≈0.1 eV. This finding is in accord with the different spectroscopic signature for O in subsurface locations: 53 meV, suitable for AgO, on Ag(210) and 68 meV, suitable for Ag_2O, on Ag(511) [49].

Furthermore, as deduced from DFT calculations, oxygen can occupy both tetrahedral and octahedral interstitials on Ag(111) [11], whereas only octahedral sites are stable on Ag(100) [22]. Such a pattern of subsurface site occupation resembles the Tasker's requirements for the stability of ionic surfaces [50]. Namely, among the low index Miller surfaces of Ag_2O (with O atoms in tetrahedral interstitials) only the (111) face has no net dipole moment perpendicular to the surface, being then a stable Tasker's type-2 surface. Ideal $Ag_2O(100)$ and $Ag_2O(110)$ are Tasker's type-3 polar surfaces and are therefore unstable. In contrast, if O atoms are located in octahedral interstitials (as in AgO) the (111) face is an unstable Tasker's type-3 surface, whereas (100) and (110) are stable Tasker's type-1 surfaces. In addition, the presence of steps and the relaxation allowed by the very limited width of the nanoterraces proved to be essential for the population of subsurface sites. This may suggest that on open vicinal surfaces with (100) and (110) exposed facets O will occupy octahedral interstitials, whereas (111) facets are required for tetrahedral site occupation.

We can therefore draw a unitary picture of the initial stages of the oxidation process at silver surfaces. When it starts at steps with an open geometry, an AgO-like phase forms with oxygens sitting in octahedral interstitials, while if the steps are close packed, occupation of both distorted tetrahedral and octahedral sites occurs and Ag_2O-like phase nucleates.

5. Conclusion

The interaction of oxygen with the Ag(511) surface, consisting of (100) terraces and (111)-like monatomic steps, was investigated experimentally by means of HREELS and photoemission spectroscopy while the energetics of the system was calculated by DFT. Four supersurface adsorption sites were identified and characterized with respect to their vibrational and photoemission signature. Moreover, we find that population of subsurface octahedral and tetrahedral sites occurs upon annealing to 200 K and that an Ag_2O-like phase, witnessed by a vibrational loss at 68 meV, nucleates at close-packed steps. Such behaviour is at variance with that observed for O/Ag(210), for which surface only off-centre octahedral sites are occupied by O atoms and an AgO-like phase vibrating at 53 meV forms. This demonstrates that the stoichiometry of the surface oxide phase is tuned by the geometry of the steps, at least in the early stages of oxide formation. For both surfaces, incorporation is enabled by the large lattice relaxation associated with the small terrace width, which reduces the energetic cost for lattice deformation.

Acknowledgments

We acknowledge funding by Compagnia S Paolo and by the Ministry of Foreign Affaires through a bilateral agreement between Italy and Slovenia. We thank Antoine Hinaut for collaborating in the last part of the experiments.

References

[1] Van Santen R A and Kuipers H P C 1987 *Adv. Catal.* **35** 265
[2] Campbell C T 1985 *Surf. Sci.* **157** 43
[3] Rocca M 1996 *Phys. Scr.* T **66** 262
[4] Savio L, Vattuone L and Rocca M 2001 *Phys. Rev. Lett.* **87** 276101
[5] Vattuone L, Savio L and Rocca M 2003 *Phys. Rev. Lett.* **90** 228302

[8] No 528.1 eV O moiety was reported in [43] since XPS was systematically recorded after HREELS inspection and this peak is rapidly removed by the residual CO of the UHV chamber.

[6] Kokalj A, Bonini N, Dal Corso A, de Gironcoli S and Baroni S 2004 *Surf. Sci.* **566–568** 1107
[7] Bonini N, Dal Corso A, Kokalj A, de Gironcoli S and Baroni S 2005 *Surf. Sci.* **587** 50
[8] Vattuone L, Burghaus U, Savio L, Rocca M, Costantini G, Buatier de Mongeot F, Rusponi S, Boragno C and Valbusa U 2001 *J. Chem. Phys.* **115** 3346
[9] Rovida G, Pratesi F, Maglietta M and Ferroni E 1972 *J. Vac. Sci. Technol.* **9** 796
[10] Todorova M, Li W X, Ganduglia-Pirovano M V, Stampfl C, Reuter K and Scheffler M 2002 *Phys. Rev. Lett.* **89** 96103
[11] Li W X, Stampfl C and Scheffler M 2003 *Phys. Rev.* B **67** 045408
[12] Michaelides A, Bocquet M L, Sautet P, Alavi A and King D A 2003 *Chem. Phys. Lett.* **367** 344
[13] Schmidt M, Masson A and Brechignac C 2003 *Phys. Rev. Lett.* **91** 243401
[14] Waterhouse G I N, Bowmaker G A and Metson J B 2001 *Appl. Surf. Sci.* **183** 191
[15] Over H *et al* 2000 *Science* **287** 1474
[16] Hendriksen B L M and Frenken J W M 2002 *Phys. Rev. Lett.* **89** 046101
[17] Chiu Y, Rambabu U, Hsu M-H, Hang-Ping D Shieh, Chen C-Y and Lin H H 2003 *J. Appl. Phys.* **94** 1996
[18] Schnadt J, Michaelides A, Knudsen J, Vang R T, Reuter K, Lægsgaard E, Scheffler M and Besenbacher F 2006 *Phys. Rev. Lett.* **96** 146101
[19] Schmid M, Reicho A, Stierle A, Costina I, Klikovits J, Kostelnik P, Dubay O, Kresse G, Gustafson J, Lundgren E, Andersen J N, Dosch H and Varga P 2006 *Phys. Rev. Lett.* **96** 146102
[20] Li W-X, Stampfl C and Scheffler M 2003 *Phys. Rev.* B **68** 165412
[21] Carlisle C I, Fujimoto T, Sim W S and King D A 2000 *Surf. Sci.* **470** 15
[22] Kokalj A, Dal Corso A, de Gironcoli S and Baroni S 2006 *J. Phys. Chem.* B **110** 367
[23] Yvon K, Bezinge A, Tissot P and Fischer P 1986 *J. Solid State Chem.* **65** 225
[24] Pettinger B *et al* 1994 *Angew. Chem. Int. Edn* **33** 85
[25] Rocca M *et al* 2000 *Phys. Rev.* B **61** 213
[26] Vattuone L *et al* 1995 *J. Chem. Phys.* **101** 713
[27] Loffreda D *et al* 2003 *Surf. Sci.* **530** 26
[28] Savio L *et al* 2006 *J. Phys. Chem.* B **110** 942
[29] Campbell C T and Paffett M T 1984 *Surf. Sci.* **143** 517
[30] Tjeng L H *et al* 1990 *Phys. Rev.* B **41** 3190
[31] Rocca M *et al* 2001 *Phys. Rev.* B **63** 081404
[32] Bao X, Muhler M, Schedel-Niedrig Th and Schloegl R 1996 *Phys. Rev.* B **54** 2249
[33] Savio L *et al* 2002 *Surf. Sci.* **506** 213
[34] Bukhiyarov V I, Kaichev V V and Prosvirin I P 1999 *J. Chem. Phys.* **111** 2169
[35] Bao X, Muhler M, Pettinger B, Schloegl R and Ertl G 1993 *Cat. Lett.* **22** 215
[36] Citrin P H, Wertheim G K and Baer Y 1983 *Phys. Rev.* B **27** 3160
[37] Wagner C D *et al* 1981 *Surf. Interface Anal.* **3** 221
[38] Perdew J P, Burke K and Ernzerhof M 1996 *Phys. Rev. Lett.* **77** 3865
[39] Vanderbilt D 1990 *Phys. Rev.* B **41** 7892
[40] Baroni S, Dal Corso A, de Gironcoli S, Giannozzi P, Cavazzoni C, Ballabio G, Scandolo S, Chiarotti G, Focher P, Pasquarello A, Laasonen K, Trave A, Car R, Marzari N and Kokalj A Code available from http://www.pwscf.org/
[41] Kokalj A 2003 *Comput. Mater. Sci.* **28** 155 Code available from: http://www.xcrysden.org/
[42] Vattuone L, Gambardella G, Valbusa U and Rocca M 1997 *Surf. Sci.* **378/379** 671
[43] Savio L, Vattuone L and Rocca M 2007 *Appl. Phys.* A **87** 399
[44] Savio L *et al* 2005 *Chem. Phys. Lett.* **404** 336
[45] Zemlyanov D Y, Savinova E, Scheybal A, Doblhofer K and Schlogl R 1998 *Surf. Sci.* **418** 441
[46] Benedek G *et al* 2001 *Europhys. Lett.* **53** 544
[47] Savio L, Gerbi A, Vattuone L, Raghani P, Bonini N, de Gironcoli S and Rocca M 2007 *J. Phys. Chem.* C **111** 10923
[48] Bonini N, Kokalj A, Dal Corso A, de Gironcoli S and Baroni S 2004 *Phys. Rev.* B **69** 195401
[49] Savio L, Giallombardo C, Vattuone L, Kokalj T and Rocca M 2008 to be submitted
[50] Tasker P W 1979 *J. Phys. C: Solid State Phys.* **12** 4977